AERODYNAMIC ROUGHNESS AND SALTATION TRAPPING EFFICIENCY OF TILLAGE RIDGES

L. J. Hagen, D. V. Armbrust
MEMBER ASAE MEMBER ASAE

ABSTRACT

A new wind erosion prediction system (WEPS) is being developed by a modeling team to replace the current wind erosion equation. WEPS simulates erosion, as well as soil and biomass conditions that control wind erosion. Parameters for the WEPS erosion submodel are being developed in a series of wind tunnel experiments. Field tillage ridges containing large aggregates are often used to aid in control of wind erosion. Two of the ways armored ridges control erosion are raising the threshold velocity where erosion begins and trapping saltating soil particles. The objectives of this study were to determine:

a) aerodynamic roughness length and displacement height of tillage ridges,
b) static and dynamic threshold friction velocities of armored ridges, and
c) ridge trapping efficiency.

Eight sets of simulated tillage ridges, ranging from 23.7 to 150 mm in height and armored with 2 to 6 mm gravel, were installed over 6.1 m of a wind tunnel working section and tested. Using wind speed profile measurements, estimating equations were developed to predict ridge aerodynamic roughness length and displacement height as functions of ridge height and ratio of ridge height to along-wind ridge spacing. Estimating equations also were developed to predict both static and dynamic threshold friction velocities as functions of ridge aerodynamic roughness length. From measurements of depletion of saltation discharge passing over the ridges, an estimating equation was developed to predict ridge trapping efficiency as a function of saltation discharge, saltation discharge transport capacity, and ridge geometry.

KEYWORDS. Tillage, Erosion, WEPS.

INTRODUCTION

A modeling team in the United States Department of Agriculture is developing technology to replace the current wind erosion equation (Woodruff and Siddoway, 1965) with a computer model, dubbed WEPS for Wind Erosion Prediction System. WEPS simulates erosion, as well as the weather, hydrology, soil, tillage, and biomass conditions that control wind erosion (Hagen, 1991a). Experiments to develop parameters for the erosion submodel of WEPS are being carried out in a series of wind tunnel studies. This article reports the results of a wind tunnel experiment on simulated tillage ridges.

Wind erosion on agricultural soils is composed of several subprocesses (Hagen, 1991b). These can be modeled as a series of sources and sinks, which control the amount of soil mass moving in the saltation and creep transport modes, using the principle of mass conservation (fig. 1). The subprocesses are emission of loose aggregates from among the large clods by wind and impact of saltating aggregates, trapping (deposition) of saltation and creep in sheltered areas, suspension of fine particles from emission and abrasion, and finally, the abrasive breakdown of aggregates or crust to wind-erodible size. Tillage ridges are often used as part of wind erosion control systems. Indeed, when vegetation is removed for food, fiber, fuel, or fodder, ridges and soil aggregation are frequently the only means used to control wind erosion on large areas.

From inspection of figure 1 and a review of the literature, a qualitative understanding of the ways tillage ridges affect wind erosion can be obtained. First, ridges generally increase aerodynamic surface roughness, so that for a given outdoor geostrophic wind velocity (freestream in the wind tunnel), surface friction velocity is larger on a ridged surface than on an unridged surface. Thus, for meaningful comparisons of ridged and unridged surfaces in the outdoors, one must use equivalent geostrophic wind velocities and convert these to friction velocities, rather than initially select equivalent friction velocities, as is typical in the literature. Further, the threshold wind speed at which ridge tops composed of loose, erodible-size material erode will be less than that at which an unridged surface erodes. However, emission of loose soil will cause

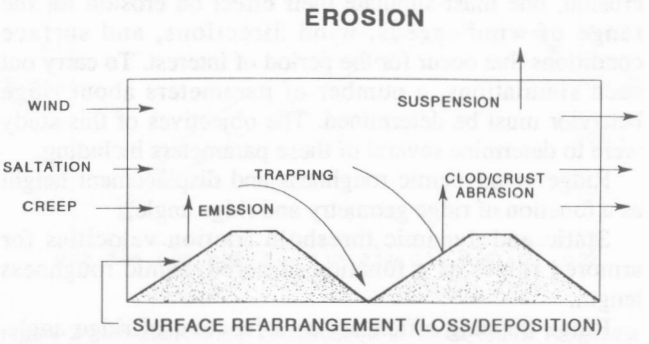

Figure 1–Diagram of a control volume for the erosion submodel with bare soil illustrating sources and sinks for moving soil.

Article was submitted for publication in January 1992; reviewed and approved for publication by the Soil and Water Div. of ASAE in June 1992.

Contribution from USDA-Agricultural Research Service, in cooperation with Kansas Agricultural Experiment Station. Contribution Number 91-458-J.

The authors are **Lawrence J. Hagen**, Agricultural Engineer, and **Dean V. Armbrust**, Soil Scientist, USDA-Agricultural Research Service, Kansas State University, Manhattan.

ridge tops containing large clods to quickly armor, so loose soil can be emitted only from the ridge troughs. In the latter case, threshold wind speed will be above that for the unridged surface, except for winds parallel to the ridges.

Although the upper part of the windward ridge face has high shear stress, other regions experience less shear than unridged surfaces (Zilker and Hanratty, 1979). The distribution of surface shear stress is also reflected in the emission of loose soil. Loss of loose sand from simulated tillage ridges 10 to 200 mm tall composed of mixtures of sand and gravel was measured from a 1.62 m long tray in the wind tunnel (Armbrust et al., 1964). Ridges upwind from the tray were armored, so that losses from the downwind tray represented emission with very little trapping. The results showed that at equal friction velocities, ridges often reduced total emission up to 50% compared to unridged surfaces.

In another wind tunnel study (Fryrear, 1984), simulated tillage ridges were constructed from rough masonite over an entire 7 m tunnel test section and covered with 10 mm of erodible (< 0.42 mm) soil. Next, the soil was left uncovered or covered with 20%, 40%, and 60% non-abradable, simulated aggregates. In this study, soil emitted from ridge tops had to cross several ridges before exiting the tunnel. Thus, both emission and trapping were active subprocesses. The results showed that at equal friction velocities, ridges reduced soil loss from the surface 89% to 98% compared to unridged surfaces. Obviously, these results are dependent on test wind speeds and even tunnel test length, as well as other variables. Nevertheless, the results demonstrated that trapping is an important subprocess in ridged fields.

The abrasion process on ridges will be most active on the windward ridge face, which is typically armored with clods or crust. Vertical profiles of the saltation discharge over ridges show that the upper portion of the ridge receives most of the impacts, with reduced flux in the lower trough area (Hagen and Armbrust, 1985). The amount of abrasion loss depends mainly on the saltation discharge and the abrasion resistance of the target clods and crust (Hagen, 1984; Hagen, 1991b). Crusts have lower abrasion resistance than clods, and both can vary widely. Crust abrasion coefficients for a range of soils have been measured (Zobeck, 1991). Trapping of saltating soil also exerts a strong influence on abrasion loss, because downwind abrasion loss is reduced in direct proportion to the upwind amount of soil trapped.

In order to fully assess the effect of ridges on wind erosion, one must simulate their effect on erosion for the range of wind speeds, wind directions, and surface conditions that occur for the period of interest. To carry out such simulations, a number of parameters about ridge behavior must be determined. The objectives of this study were to determine several of these parameters including:

Ridge aerodynamic roughness and displacement height as a function of ridge geometry and ridge angle,

Static and dynamic threshold friction velocities for armored ridges as a function of aerodynamic roughness length.

Ridge trapping efficiency as a function of ridge angle, ridge geometry, saltation discharge, and saltation discharge transport capacity.

Experimental Procedure

Simulated tillage ridges composed of a mixture of 2 to 6 mm diameter gravel and 0.29 to 0.42 mm quartz sand were constructed normal or angled to the flow in the working section of a recirculating wind tunnel. The tunnel has a 7 m working section, which is 0.76 m wide and 0.91 m tall. For each test, a downwind 6.1 m length of working section of tunnel floor was covered with ridges, and the tunnel roof was adjusted to give zero pressure gradient along the working section. The ridges were constructed by filling a wooden, triangular form, which was open at the apex.

Boundary layer wind speed profiles were measured at a location near the downwind end of the tunnel and centered between ridge peaks using a pitot-static tube. Freestream wind speeds also were measured simultaneously using a second pitot-static tube. Profile data using two freestream wind speeds were collected for each set of test ridges. These data were analyzed, using the methods of Ling (1976), to determine aerodynamic parameters without saltation for the ridges as defined by the log-law wind speed profile in the lower portion of the boundary layer. The log-law profile was generally present in a zone extending from 0.8 to 1.5 ridge heights above the surface of the troughs. There were more than 10 data points in the log-law region for each profile. The log-law wind speed profile (Panofsky and Dutton, 1984) is defined as:

$$U = \left(\frac{U*}{k}\right) Ln\left(\frac{(Z-D)}{Z_o}\right) \quad (1)$$

where $U*_{is}$ friction velocity (LT^{-1}), k is a constant (0.4), Z is height above the ridge trough (L), D is displacement height above ridge trough (L), and Z_o is aerodynamic roughness length (L).

After measurement of aerodynamic roughness, trapping efficiency was measured for each set of ridges using the following procedures. First, the loose soil on the ridge tops was removed by operating the tunnel until the ridges were armored on the upwind sides. Thus, during the trapping experiments, the abrasion, emission, and suspension flux components were zero (fig. 1). Next, a weighed amount of sand (0.29 to 0.42 mm diameter) was placed in a uniform bed across the tunnel floor upwind from the ridges, and the tunnel operated for three to five minutes with a relatively constant saltation discharge entering the ridges. At the downwind side of the ridges, a vertical slot sampler collected the saltating sand in a pan mounted on a recording load cell below the tunnel floor. Finally, the remaining sand on the floor upwind was reweighed, and the loss was compared to the flux that had passed the sampler. Measurements, prior to the ridge tests, showed sampler efficiency was 0.89. The difference was the sand trapped by the ridges.

To calculate ridge trapping efficiency (T_e), the ridges were assumed to act like a series of filters operating in a quasi-steady state during each test run. A summary of the mechanisms by which fitters remove particles from a gaseous airstream is presented by Lodge (1989). Using conservation of mass principles, a series of filters can be modeled as:

$$\frac{dq}{dx} = -T_e q \qquad (2)$$

Integrating equation 2 gives:

$$T_e = [1/L_x] \, Ln\left(\frac{Q_{in}}{Q_{out}}\right) \qquad (3)$$

where q is saltation discharge in the downwind, x-direction ($ML^{-1}T^{-1}$), Q is the test run-time integral of q (ML^{-1}), and L_x is the ridge-covered tunnel length (L).

Because T_e is a function of q, equation 2 is valid only when the variation of q over the test bed is small, i.e., for test conditions where T_e is relatively low. Each set of ridges was tested at three freestream wind speeds. For the two highest wind speeds a second saltation discharge rate was created by adding a low wire screen barrier in front of the upwind sand source.

The surface contour of each set of ridges was measured over one or two wavelengths by lowering a laser beam, which was mounted parallel with the ridge surface, until it intercepted the surface. The relative change in height from a scale fastened to the laser optics was then measured for several positions along the ridge profile. The characteristics of the tested ridges are listed in Table 1,
where H is ridge height and H/L is ridge height to spacing ratio along the wind direction.

Static threshold friction velocities also were determined on several of the ridge sets as follows: The troughs were filled with 0.29 to 0.42 mm sand and blown until they reached static equilibrium (q = 0) at 15.5 ms^{-1} freestream wind speed. Ridge characteristics were then measured with the laser as previously described.

Results and Discussion

Aerodynamic Roughness Parameters

Aerodynamic roughness parameters, Z_o and D, were calculated from the wind speed profiles in the lower part of the boundary layer using an iterative procedure. First, initial values for D were selected, then multiple wind speed profiles for each ridge set were analyzed to calculate Z_o using the least-squares technique recommended by Ling (1976). Successive values of D were selected to maximize R^2 of the least-squares fit to the profile. Finally, the results were scaled by ridge height (H) and ridge spacing along the wind direction (L) (fig. 2).

TABLE 1. Characteristics of ridges used in aerodynamic and trapping tests.

H/L	H (mm)	Range of q (kg $M^{-1}s^{-1}$)	Range of U_* (ms^{-1})	Ridge Angle (deg)
0.21	45.2	0.011 - 0.044	0.78 - 1.12	90
0.18*	76.0	0.018 - 0.052	0.97 - 1.38	90
0.15	64.5	0.007 - 0.089	0.92 - 1.26	90
0.11*	47.3	0.010 - 0.048	0.72 - 1.14	90
0.11*	23.7	0.025 - 0.054	0.71 - 0.93	90
0.067	105.0	0.002 - 0.052	0.81 - 1.13	16
0.056*	45.0	0.006 - 0.066	0.63 - 0.95	13
0.046	150.0	0.001 - 0.019	0.83 - 1.24	11

* Ridges used in static threshold tests.

The values for D/H ranged from 0.08 to 0.52. In general, D is caused by the reversed flow zone in the ridge trough. As H/L approaches 0.033, the reversed zone caused by flow separation is no longer present (Zilker and Hanratty, 1979). Consequently, as H/L approaches 0.033, D/H must approach the D/H value of the unridged surface. As H/L approached 0.2, D/H reached 0.5, which is in agreement with the values reported in other studies (Buckles et al., 1984). Between the upper and lower limits, the variation in D/H could be described by the equation:

$$\frac{D}{H} = 0.94 + 0.27 \, Ln\left(\frac{H}{L}\right), \quad R^2 = 1.0 \qquad (4)$$

Similar to the behavior of D/H at low values of H/L, Z_o also approached the roughness values for the unridged surface. As the values of H/L increased, however, the values for Z_o/H appeared to peak at 0.11 near H/L equal 0.18. This result also follows the commonly observed principle that as the number of surface elements increases beyond some value, the aerodynamic surface roughness tends to decrease (Shaw and Pereira, 1982). An estimating equation to predict Z_o based on calculated values is:

$$\frac{Z_o}{H} = 0.006 + 0.433\left(\frac{H}{L}\right) + 4.764\left(\frac{H}{L}\right)^2 - 20.650\left(\frac{H}{L}\right)^3, \quad R^2 = 0.97 \qquad (5)$$

When the distance L was calculated along the wind direction rather than peak-to-peak for angled ridges, they conformed to the same roughness and displacement pattern as the ridges normal to the wind. However, this result needs further confirmation in outdoor studies, because outdoor winds have larger lateral variance than tunnel winds.

Static and Dynamic Threshold Friction Velocities

The conventional application of the terms static and dynamic friction velocity has been to all-erodible surfaces composed of particles of a single size (Greeley and Iverson, 1985). In this study, the meaning was extended to armored ridges with erodible sand (0.29 to 0.42 mm) in the

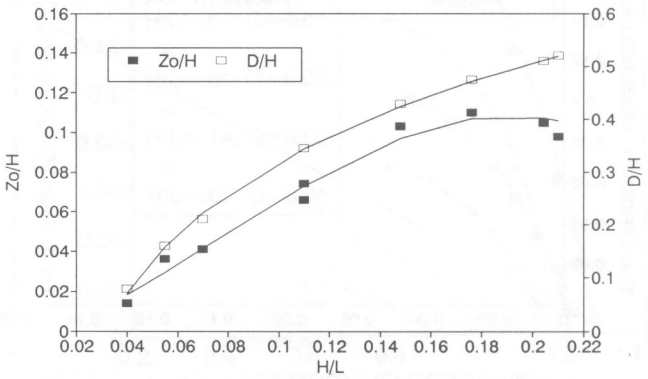

Figure 2–Non-dimensional relationships of aerodynamic roughness length (Z_o/H) and displacement height (D/H) to ridge height-to-spacing ratio (H/L).

bottom of the trough. Further, when sand was saltating across the ridges and both emission and T_e were zero, that condition was defined as the transport capacity (q_c) for a given $U*$ and ridge geometry. For each ridge set, a value of dynamic threshold friction velocity was selected to maximize the R^2 of a linear relationship between Te and $(q - q_c)$, as illustrated in figure 3 for ridges with H/L equal 0.18. Values for q_c were calculated using the equation:

$$q_c = U*^2 \frac{(U* - U*_{td})}{3.15}, \qquad U*_{td} > 0.67\, U* \qquad (6)$$

where $U*_{td}$ equals dynamic threshold friction velocity (LT^{-1}). The assumption of a linear relationship is questionable for large values of T_e, but it appeared to fit the data for T_e less than 0.15 m^{-1}. During some tests, $U*$ was less than $U*_{td}$ and caused a negative q_c. Using negative q_c values, rather than zero, greatly improved the linear relationship between T_e and $(q - q_c)$.

The calculated dynamic ridge threshold friction velocities tended to approach the ridge static values, as the ridge aerodynamic roughness increased (fig. 4). However, at low values of Z_o, the ridge tended to approach the conventional dynamic prediction curve, which was plotted as 80% of the measured static values. The probable reason for this behavior stems from the impact angle of the saltating grains. As Z_o increases and H/L exceeds 0.11, the lee separation zone begins to be sheltered from direct grain impacts, which average about 12° (Hagen, 1991b). Thus, as roughness increases, most sand grains leaving the separation zone must leave without the benefit of direct impacts, i.e., under static conditions.

The predicted static values followed nearly a quadratic semi-log relationship given by:

$$U*_{ts} = 0.84 + 0.208\,\mathrm{Ln}(Z_o) + 0.0205\,(\mathrm{Ln}(Z_o))^2$$

$$R^2 = 1.0 \qquad (7)$$

where $U*_{ts}$ equals static friction velocity of armored ridges (LT^{-1}).

The dynamic friction velocity values follow the relationship:

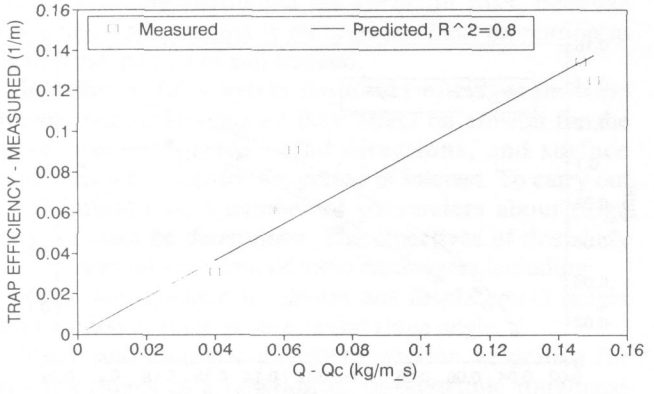

Figure 3–Measured ridge trapping efficiency as a function of difference between saltation discharge and saltation discharge transport capacity ($Q - Q_c$) for ridges with height-to-spacing ratio of 0.18.

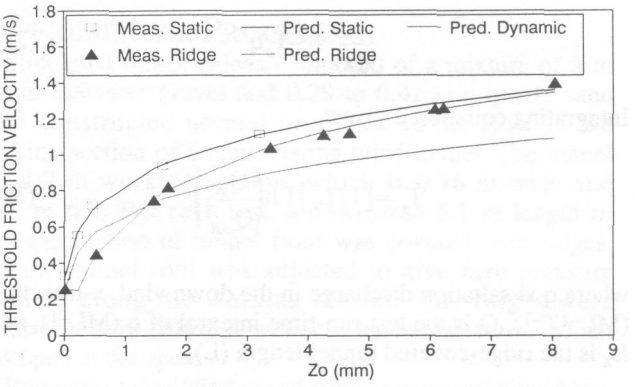

Figure 4–Static and dynamic friction velocities as a function of aerodynamic roughness length (Z_o).

$$U*_{td} = 0.632 + 0.31\,\mathrm{Ln}(Z_o) + 0.028\,(\mathrm{Ln}(Z_o))^2$$

$$-0.00564\,(\mathrm{Ln}(Z_o))^3, \qquad R^2 = 1.0 \qquad (8)$$

The single point below the conventional dynamic prediction was for an angled ridged surface where the surface wind may have tended to follow the trough and reduce the effective roughness. The lowest static and dynamic velocities on figure 4 are values for an unridged surface.

As noted in the introduction, ridged fields have higher friction velocities than unridged fields. Thus, for realistic comparisons, one needs an estimate of the ratio of the two friction velocities at a fixed geostrophic wind speed. Panofsky and Dutton (1984) reported an approximate relation of surface friction velocity and geostrophic winds, based on an analysis by Blackadar. For neutral stability and strong winds, a numerical analysis of the Panofsky and Dutton relation resulted in the following approximation:

$$\frac{U*_r}{U*_s} = \frac{1.0078\, Z_{or}^{0.0703}}{Z_{os}^{0.0708}} \qquad (9)$$

where

$U*_r$ = friction velocity for surface with largest roughness (LT^{-1})

$U*_s$ = friction velocity for surface with smallest roughness (LT^{-1})

Z_{or} = roughness length for surface with largest roughness (L)

Z_{os} = roughness length for surface with smallest roughness (L)

Thus, in simulations of erosion, to compare effects of an unridged surface of Z_{os} = 1.0 mm at a windspeed, $U*_s$ = 1 ms^{-1}, to those of a ridged surface with Z_{or} = 10 mm, one should use $U*_r$ = 1.18 ms^{-1}.

Ridge Trapping Efficiency

As illustrated in figure 3, trapping efficiency of individual ridge sets at low T_e can be described by the equation:

$$T_e = B(q - q_c) \qquad (10)$$

Values of the coefficient, B, also were computed from the data and varied as a function of ridge geometry, where:

$$B = 1.344\left(\frac{H}{L}\right) - 11.348\left(\frac{H}{L}\right)^2 + 49.643\left(\frac{H}{L}\right)^3 - 53.827\left(\frac{H}{L}\right)^4 \quad (11)$$

B increases with H/L, because the relative size of the reversed flow zone where particles are easily trapped also increases with H/L (Zilker and Hanratty, 1979). After removal from the data set of runs in which emission occurred, there were 53 trapping runs, and equation 10 was used to compute predicted values for comparison with observed values (fig. 5). The data exhibited symmetric scatter about the 1:1 line and a zero intercept and had an $R^2 = 0.8$.

Predictions of the T_e using equation 10 for various 150 mm-high ridges under low and high saltation discharge illustrate that T_e is sensitive to both $U*$ and q, whenever q exceeds q_c (fig. 6). Predictions of T_e for small ridges (H = 50 mm) illustrate a somewhat lower sensitivity to friction velocity than the large ridges (fig. 7).

For a series of ridges, the trapping flux along the wind direction is given by:

$$\frac{dq}{dx} = -B(q - q_c)\,q \quad (12)$$

Integrating equation 12 gives

$$W = \mathrm{Ln}\left(\left(\frac{Q_{out}}{Q_{in}}\right)\left(\frac{Q_{in} - q_c}{Q_{out} - q_c}\right)\right) / \left(Bq_c\right) \quad (13)$$

where

Q_{out} = saltation discharge exiting a series of trapping ridges at distance L downwind ($ML^{-1}T^{-1}$)

Q_{in} = saltation discharge entering a series of trapping ridges ($ML^{-1}T^{-1}$)

W = width of trapping strip along wind direction

As an example, consider a saltation discharge entering a trap strip of armored ridges created by emergency tillage, which partly fill over time, where

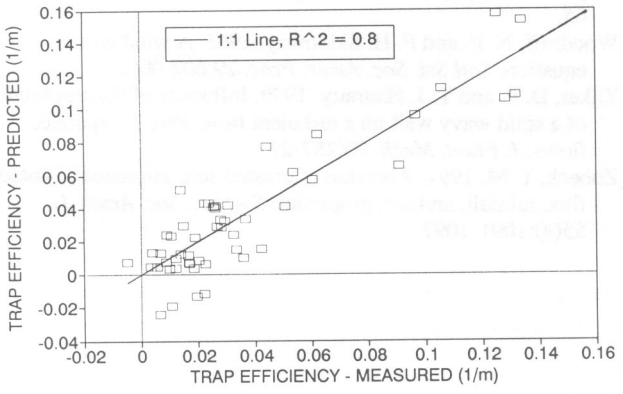

Figure 5–Predicted ridge trapping efficiency versus trapping efficiency measured in wind tunnel tests.

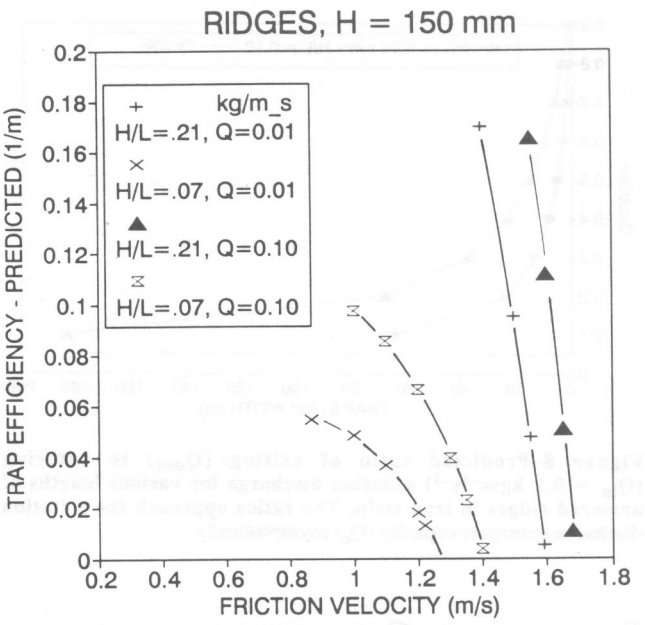

Figure 6–Predicted trapping efficiencies of 150 mm tall ridges for a range of height-to-spacing ratios, saltation discharges, and friction velocities.

Q_{in} = 0.1 $kgm^{-1}s^{-1}$

H/L = 0.25 initial condition

H/L = 0.1 after partial filling

q_c = 0.005 $kgm^{-1}s^{-1}$

The results show that 80% of the entering soil is trapped in widths of 24 and 68 m of ridges for H/L = 0.25 and 0.1, respectively (fig. 8). The results illustrate the importance of ridge geometry and adequate strip width, particularly in high winds where qc is greater than zero.

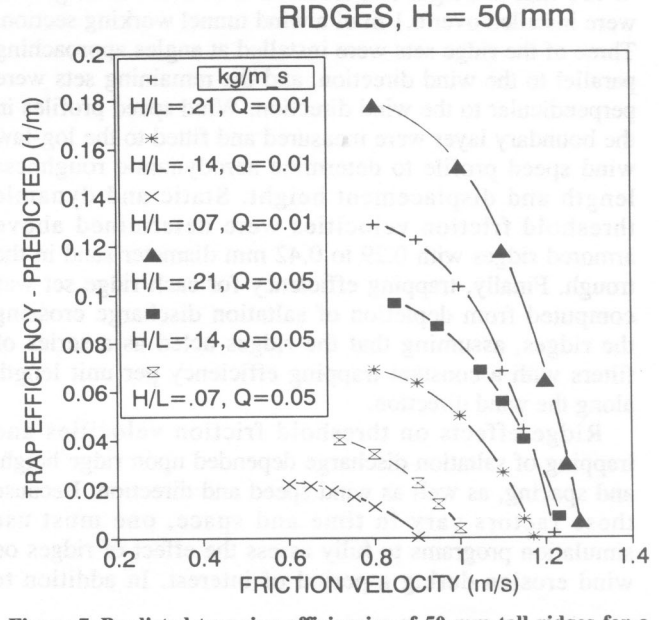

Figure 7–Predicted trapping efficiencies of 50 mm tall ridges for a range of height-to-spacing ratios, saltation discharges, and friction velocities.

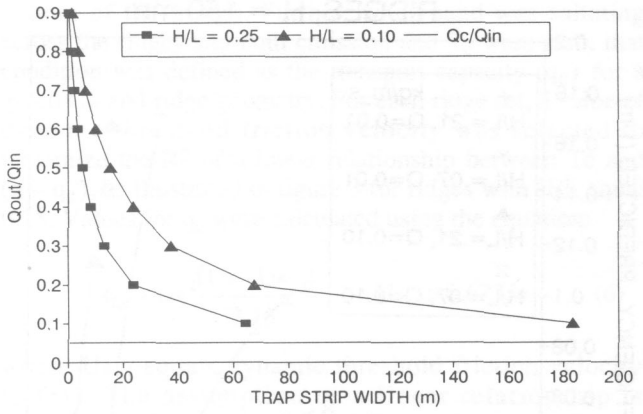

Figure 8–Predicted ratio of exiting (Q_{out}) to entering (Q_{in} = 0.1 $kgm^{-1}s^{-1}$) saltation discharge for various lengths of armored ridges in trap strip. The ratios approach the saltation discharge transport capacity (Q_c) asymptotically.

Summary and Conclusions

A new wind erosion prediction system (WEPS) is being developed, which simulates wind erosion, as well as the soil and biomass conditions that control wind erosion. In the WEPS erosion submodel, wind erosion is being modeled as a series of sources and sinks that control the amount of soil mass moving in the saltation and creep transport modes, using the principle of mass conservation. One of the major sinks for moving soil is trapping between tillage ridges. For use in the WEPS erosion submodel, a wind tunnel experiment was carried out to determine some parameters of tillage ridges which that control their effects on erosion. The objectives of this study were to determine: a) aerodynamic roughness length and displacement height of tillage ridges; b) static and dynamic threshold friction velocities of armored ridges; and c) ridge trapping efficiency for saltation discharge.

Eight sets of simulated tillage ridges, ranging from 23.7 to 150 mm in height and armored with 2 to 6 mm gravel, were installed over 6.1 m of a wind tunnel working section. Three of the ridge sets were installed at angles approaching parallel to the wind direction, and the remaining sets were perpendicular to the wind direction. Wind speed profiles in the boundary layer were measured and fitted to the log-law wind speed profile to determine aerodynamic roughness length and displacement height. Static and dynamic threshold friction velocities were determined above armored ridges with 0.29 to 0.42 mm diameter sand in the trough. Finally, trapping efficiency for each ridge set was computed from depletion of saltation discharge crossing the ridges, assuming that the ridges acted as a series of filters with a constant trapping efficiency per unit length along the wind direction.

Ridge effects on threshold friction velocities and trapping of saltation discharge depended upon ridge height and spacing, as well as wind speed and direction. Because these factors vary in time and space, one must use simulation programs to fully assess the effect of ridges on wind erosion during a period of interest. In addition to trapping and threshold velocities, one must also consider two sources, emission and abrasion, and an additional sink, suspension loss, in simulations. Future work will deal with complete numerical simulation of ridges in a range of climates.

Nevertheless, the present results can be used for some limited practical applications. The static threshold friction velocities of armored ridges are large. Further, equations 1, 5, 7, and 9, can be used to compute the threshold wind speed at a nearby weather station. As an example, for a station anemometer height = 10 m, Z_o = 5 mm, results show that ridges 50 and 200 mm high with wind angles greater than 15° have threshold wind velocities greater than 19 and 24 ms^{-1}, respectively.

In special cases, such as emergency tillage, the major subprocess operating in the tilled trap strip may be trapping of incoming saltation discharge. In this case, equation 13 can be used to evaluate the design of the trap strip for a range of ridge conditions, strip widths, wind speeds, and wind directions.

References

Armbrust, D. V., W. S. Chepil and F.H. Siddoway. 1964. Effects of ridges on erosion of soil by wind. *Soil Sci. Soc. Amer. Proc.* 28:557-560.

Buckles, J., T. J. Hanratty and R. J. Adrian. 1984. Turbulent flow over large-amplitude wavy surfaces. *J. Fluid Mech.* 140:27-44.

Fryrear, D. W. 1984. Soil ridges-clods and wind erosion. *Transactions of the ASAE* 27(2):445-448.

Greeley, R. and J. D. Iverson. 1985. *Wind as a Geological Process*. New York: Cambridge University Press.

Hagen, L. J. 1991a. A wind erosion prediction system to meet user needs. *J. Soil and Water Conservation* 46(2):105-111.

———. 1991b. Wind erosion mechanics: abrasion of an aggregated soil. *Transactions of the ASAE* 34(3):831-837.

———. 1984. Soil aggregate abrasion by impacting sand and soil particles. *Transactions of the ASAE* 27(3):805-808.

Hagen, L. J. and D. V. Armbrust. 1985. Effects of field ridges on soil transport by wind. *Proc. International Workshop on Physics of Blown Sands*, University of Aarhus, Denmark, 3(8):563-586.

Ling, C. H. 1976. On the calculation of surface shear stress using the profile method. *J. Geophys. Res.* 15:2581-2582.

Lodge, J. P., Jr. 1989. *Methods of Air Sampling and Analysis*, 3rd Ed. Chelsea, MI: Lewis Publishers, Inc.

Panofsky, H. A. and J. A. Dutton. 1984. *Atmospheric Turbulence*. New York: John Wiley & Sons.

Shaw, R. H. and A. R. Pereira. 1982. Aerodynamic roughness of a plant canopy: A numerical experiment. *Agric. Meteorol.* 26:51-65.

Woodruff, N. P. and F. H. Siddoway. 1965. A wind erosion equation. *Soil Sci. Soc. Amer. Proc.* 29:602-608.

Zilker, D. P. and T. J. Hanratty. 1979. Influence of the amplitude of a solid wavy wall on a turbulent flow. Part 2. Separated flows. *J. Fluid. Mech.* 90:257-271.

Zobeck, T. M. 1991. Abrasion of crusted soil: influence of abrader flux, rainfall, and soil properties. *Soil Sci. Soc. Amer. J.* 55(4):1091-1097.